Copyright © 1984, by the author(s).
All rights reserved.

Permission to make digital or hard copies of all or part of this work for personal or classroom use is granted without fee provided that copies are not made or distributed for profit or commercial advantage and that copies bear this notice and the full citation on the first page. To copy otherwise, to republish, to post on servers or to redistribute to lists, requires prior specific permission.

CORRECTIONS TO QUASILINEAR DIFFUSION IN AREA PRESERVING MAPS

by

N. W. Murray, M. A. Lieberman, and A. J. Lichtenberg

Memorandum No. UCB/ERL M84/102

12 December 1984

cover sheet

CORRECTIONS TO QUASILINEAR DIFFUSION IN AREA PRESERVING MAPS

by

N. W. Murray, M. A. Lieberman and A. J. Lichtenberg

Memorandum No. UCB/ERL M84/102

12 December 1984

ELECTRONICS RESEARCH LABORATORY

College of Engineering
University of California, Berkeley
94720

title page

CORRECTIONS TO QUASILINEAR DIFFUSION IN AREA PRESERVING MAPS

N. W. Murray, M. A. Lieberman and A. J. Lichtenberg

Department of Electrical Engineering
and Computer Sciences and the
Electronics Research Laboratory
University of California,
Berkeley, CA 94720

Higher order corrections to the quasilinear diffusion coefficient are obtained for Hamiltonian maps which are locally approximated by the standard map. Using the Fermi map as an example we numerically integrate the Fokker-Planck equation for the action and compare the resulting distribution function with direct solutions of the mapping equations. The second moment of the distribution is compared with the diffusion measured in the numerical experiments. Both show oscillations (as a function of the initial velocity) similar to those found in the standard map. In addition we numerically find the invariant distribution in the Fermi map. We observe dips in the distribution of actions. We calculate the size of islands surrounding stable fixed points and show that the dips correspond to these islands. Thus chaotic orbits uniformly fill the phase space available to them.

I. Introduction

The study of non-linear dynamical systems has revealed many examples of chaotic behavior. The simplest systems in which such behavior is observed are two degree of freedom Hamiltonian systems. Two dimensional area preserving mappings which have their own Hamiltonian structure may be used to model such systems.

The motion of chaotic orbits cannot be described analytically, as one describes regular orbits. Rather than describing the detailed motion of a chaotic orbit, we would like to predict the statistical properties of families of orbits. In many problems, such as ion or electron cyclotron resonance heating, the evolution of only one of the two phase space variables, the action (or the energy), is of interest. We assume that the other variable, angle or phase, is randomised much more rapidly than the action. Based on these assumptions we describe the dynamics using a Fokker-Planck equation in action alone. The Fokker-Planck equation describes the evolution of the distribution of actions, as represented by the distribution function $f(u,n)$, where u is the action and n is the "time".

For a Hamiltonian system, the Fokker-Planck equation is specified by giving the diffusion coefficient $D(u)$. The quasilinear diffusion coefficient D_{ql} has been used by many authors[1,2] to describe the evolution of the action in an area preserving map. However there are stringent limits on the validity of the quasilinear approximation, which assumes phase randomization on each mapping iteration. Approximations to the diffusion coefficient that incorporate longer correlation times are thus of great interest. The global diffusion coefficient of the action for the standard map, which has been calculated by Rechester et

al.[3],[4] includes phase correlations over many mapping periods. In this paper we apply their results to more general maps, restricting ourselves to those maps locally approximated by the standard map.

We wish to describe the evolution of a distribution function $f(u,n)$ in the action alone. We assume that the phase evolves randomly and the evolution in action is a Markov process. In addition we assume that the change in action is small on the time scale over which the phases become random. These assumptions lead one to a Fokker-Planck equation for the action[5] :

$$\frac{\partial f(u,n)}{\partial n} = -\frac{\partial}{\partial u}\left(B(u)f(u,n)\right) + \frac{1}{2}\frac{\partial^2}{\partial u^2}\left(D(u)f(u,n)\right) , \tag{1}$$

where $D(u)$ is the local diffusion coefficient

$$D(u) = \frac{1}{\Delta n}\int du' \,(u'-u)^2 \, W_t\,(u,0;u',\Delta n) \ , \tag{2}$$

and $B(u)$ is the local friction coefficient

$$B(u) = \frac{1}{\Delta n}\int du' \,(u'-u)\, W_t\,(u,0;u',\Delta n) \ . \tag{3}$$

The transition probability $W_t\,(u,0;u',\Delta n)$ is the probability density that a particle has action u' at time Δn given that it had action u at time 0. The time Δn is assumed to be small compared to the evolution time, τ_{action}, of the action distribution function, but must be longer than the phase relaxation time, τ_{phase}. We assume that only the first and second moments of W_t are proportional to Δn and that coefficients corresponding to higher order moments vanish as $\Delta n \to 0$. For Hamiltonian systems with action-angle variables (i.e. with periodic dependence on the angles) and assuming random phases, it may be shown that[6]

$$B(u) = \frac{1}{2}\frac{dD(u)}{du}. \tag{4}$$

We are interested in radial twist mappings of the form[7]

$$\begin{aligned} u_{n+1} &= u_n + \epsilon \sin\theta_n \\ \theta_{n+1} &= \theta_n + A(u_{n+1}), \end{aligned} \tag{5}$$

which are area preserving and therefore have a Hamiltonian form. An example is the Fermi map, whose mapping equations in the surface of section phase plane are[1]

$$\begin{aligned} u_{n+1} &= u_n + \sin\psi_n \\ \psi_{n+1} &= \psi_n + \frac{2\pi M}{u_{n+1}} \pmod{2\pi} . \end{aligned} \tag{6}$$

These equations describe a model for the motion of a ball bouncing between two walls, one of which is fixed and the other oscillating sinusoidally. The action u_n is the normalized velocity of the ball just before the nth collision with the moving wall. The angle ψ_n is the phase of the moving wall just before the nth collision. The quantity $M = L/(2\pi a)$, where L is the distance between the walls, and $a << L$ is the maximum amplitude of the wall oscillation. Typically, $M >> 1$. We will choose $M = 10,000$ in all figures to illustrate features of the phase plane.

As shown in Fig. 1, the phase plane of the mapping divides naturally into three regions: (1) At low velocities phase space is predominantly stochastic, and all period one fixed points are unstable. We denote by u_s the action below which there exist no stable period one fixed points; (2) At intermediate velocities, stable islands (around elliptic fixed points) are embedded in the stochastic sea; (3) At high velocities, the motion is predominantly regular, with only thin stochastic regions near the separatrices joining hyperbolic fixed points. Regions (2) and (3) are separated by a KAM barrier. The average action (averaged over phase) at the barrier is denoted by u_b. Simple stability calculations, as well as

numerical results, give $u_a \approx (\pi M/2)^{1/2}$ and $u_b \approx 2.5u_a$. In this paper we focus our attention on the first two regions.

II. The Local Diffusion Coefficient

In order to use the Fokker-Planck equation to describe the Fermi map we must determine the diffusion coefficient D. The simplest procedure is to set $\Delta n = 1$ in (2) and assume a uniform distribution of initial phases. Averaging over the phases we find the quasilinear diffusion coefficient $D_{ql} = 1/2$, and the Fokker-Planck equation

$$\frac{\partial f(u,n)}{\partial n} = \frac{1}{4}\frac{\partial^2 f(u,n)}{\partial u^2}. \tag{7}$$

The result in (7) ignores phase correlations which may exist over many steps. An alternative procedure, which is valid in the limit of Δn large, is the Fourier path method applied by Rechester et al.[3,4] to diffusion in the standard map

$$\begin{aligned} I_{n+1} &= I_n + K\sin\theta_n \pmod{2\pi}, \\ \theta_{n+1} &= \theta_n + I_n \pmod{2\pi}. \end{aligned} \tag{8}$$

Note that, in contrast to the Fermi map, the standard map is 2π periodic in the action I. The Fourier path calculation depends on the periodicity of the standard map in action. Thus the long time diffusion is an average over the 2π interval in action, depending only on the stochasticity parameter K. To ensure that the procedure converged, a small external noise was added to the mapping (8). However, the noise can be taken equal to zero after the calculation, obtaining for $K > 2\pi$ [4]

$$D_\infty(K) = K^2\left[\frac{1}{2} - J_2(K) + J_2^2(K) + O\left(\frac{1}{K^2}\right)\right] \tag{9}$$

where D_∞ is the average long-time diffusion coefficient. For smaller K, the Fourier paths must be integrated numerically, obtaining for $K_{crit} < K < 2\pi$ the result shown in Fig. 2[4],[8] For $K < K_{crit} \approx 0.9716$ a KAM barrier exists and there is no long-time diffusion.

The Fourier path method depends on the peculiar periodicity in action of the standard map to evaluate the Fourier integrals in the limit of long times ($\Delta n \rightarrow \infty$). Because of this, the method of Fourier paths cannot be applied in the long time limit to maps without this periodicity. In principle, the long time diffusion coefficient for any map having motion bounded by KAM tori is $D_\infty \equiv 0$. However, the Fokker-Planck equation only requires an intermediate time diffusion coefficient, that is, $\tau_{action} >> \Delta n >> \tau_{phase}$ in equation (2). In addition, the standard map is a local approximation in action to a wide variety of maps. Thus the possibility arises that $D_\infty(K)$ may be used to approximate the local diffusion coefficient $D(u)$ for a general map. For those cases where the stochasticity parameter K depends on the action, $D(u)$ will depend on the action, through K.

Although this can be formally done, as we shall show below, there are some inherent limitations. For sharply peaked (in action) initial distributions, we cannot expect good agreement over short timescales between the predicted diffusion and the actual diffusion obtained by numerically iterating the mapping. Also, the presence of stable islands embedded within the stochastic sea will modify the diffusion when the timescale of interest is short compared to the timescale for extrinsic diffusion (noise) to diffuse phase points into and out of the islands. The modifications required to deal with these limitations are developed in the following sections.

To use $D_\infty(K)$ to obtain a local (in action) diffusion coefficient D for a more general map, we consider the example of the Fermi map (6). Linearizing around a given fixed point $u_l = M/l$, with l an integer and $\psi_1 = \pi$, we obtain

$$\Delta u_{n+1} = \Delta u_n - \sin\theta_n$$
$$\theta_{n+1} = \theta_n - \frac{2\pi M}{u_1^2}\Delta u_{n+1} \pmod{2\pi} .$$

Letting $K = 2\pi M/u_l^2$ and $I_n = -K\Delta u_n$ puts the map in the standard form (8) .

To use this result in finding a diffusion coefficient, we examine the Fokker-Planck equation for I:

$$\frac{\partial f(I)}{\partial t} = \frac{\partial}{\partial I}\left[\frac{1}{2}D_\infty(K)\frac{\partial f(I)}{\partial I}\right]$$

This equation is only valid for $(1/f)(\partial f/\partial I) << 1/(2\pi)$. This is because D_∞ is obtained in the long time limit, implying averaging over many 2π intervals in the action I. Correspondingly, for the Fermi map we write

$$\frac{\partial g(u)}{\partial t} = \frac{\partial}{\partial u}\left[\frac{1}{2}D(u)\frac{\partial g(u)}{\partial u}\right]$$

Since $\partial/\partial u = K(u_l)\partial/\partial I$ locally, this suggests that

$$D(u) = \frac{1}{K^2(u)}D_\infty\left(K(u)\right) . \tag{10}$$

Appendix A gives a derivation of this result. For an initial broad distribution $(1/g)(\partial g/\partial u) << K(u)/(2\pi)$ we expect (10) to yield good correspondence to the numerically determined distribution. For a sharply peaked distribution, we expect good agreement only for times exceeding the time required for the distribution to broaden over many primary resonances, $n >> 1/(K^2D) = 1/D_\infty$.

For $u < M^{1/2}$, using (9), we obtain

$$D(u) = \frac{1}{2} - J_2\left(\frac{2\pi M}{u^2}\right) + J_2^2\left(\frac{2\pi M}{u^2}\right) + O\left(K^{-2}\right) . \qquad (11)$$

For larger actions u, we apply (10) to Fig. (2). For small values of u, D oscillates rapidly around the quasilinear value $D_{ql} = 1/2$, while for large values of u it drops rapidly to zero at $K = K_{crit}$.

The calculations of Rechester et al[3,4]assume the presence of noise, enabling particles to diffuse into and out of stable islands. When the particles are in the islands, they behave as though they are trapped and do not diffuse globally. The diffusion coefficient obtained in this manner averages two populations: particles outside islands with a non-zero diffusion coefficient and particles inside islands with a negligibly small diffusion coefficient.

In this study we are primarily interested in heating problems. In such problems, particles will generally start at low velocities, where the stable islands have negligibly small area. As the particles are heated their velocities increase, and they enter regions of phase space within which large islands exist. Without extrinsic stochasticity the particles will not become trapped within the islands. Thus we are interested only in averaging the diffusion over the untrapped distribution. For an ergodic phase space, the equilibrium distribution is uniform.[9] With embedded islands one would expect that the equilibrium (infinite time) distribution in the connected portions of the phase space would also be uniform. Thus to extract the diffusion of the untrapped species, alone, from the results of Rechester et al., we divide their diffusion coefficient by the fraction of phase space occupied by stochastic orbits. We denote the stochastic population distribution by $f_s(K, I)$ and the trapped distribution function by

$f_i(K,I)$, where $f_s(K,I)+f_i(K,I)=1$. These are the equilibrium distributions for the standard map with stochasticity parameter K. We define the relevant diffusion coefficient for the Fermi map as

$$D(u)=\frac{D_\infty(K(u))}{K^2(u)<f_s(K(u_l),I(\Delta u))>_I} \tag{12}$$

where $K(u_l)=2\pi M/u_l^2$ and $I(\Delta u)=-K\Delta u$. The average over a 2π interval in I ignores rapid variations in the diffusion coefficient, which is consistent with (10). If rapid variations in D were kept, they would be smoothed rapidly in integrating the Fokker-Planck equation. Nevertheless, as we see below, the rapid variations in the distribution function must be retained.

We have investigated the correctness of this picture using the Fermi map. In appendix B we calculate the size of the last stable orbit surrounding each stable period one and period two fixed point. We use the approximation that the width of the separatrix layer surrounding the island(s) can be obtained from overlap of second order islands of the appropriate separatrix mapping[2',7] These "last" island KAM curves yield the fractions $f_s(u,M)$ (solid curves) shown in Fig. 3. The two variables u, M correspond to the variables Δu, u_l in (12). We assume a fixed M and therefore suppress the M dependence in f_s. We expect the size of the islands having fixed point periods greater than two to decrease sufficiently rapidly with period that the sum of their areas is negligible.

To compare with this analytical calculation, we have numerically calculated the equilibrium distribution function $f_s(u)$. Iterating 64 initial conditions 10 million times yields the distribution function shown as dots in Fig. 3. The action space between $u=0$ and $u=250$ was divided into 6000 bins. The height of the curve represents the total number of visits to a particular bin, suitably

normalized. The dips in $f(u,n)$ persist over a large range in the number of iterations (from $n = 10^5$ to $n = 10^7$)and do not change when a double precision calculation is made. The primary difference between the theoretical and numerical values of $f_s(u)$ is the stairstep pattern of the dips in the numerical value compared to the smooth increase in the magnitude of the dips with increasing u as determined from the perturbation calculation. The stairstep pattern in the numerical results is due to the discreteness of the second order islands. A more exact perturbation calculation has been done on a related problem, bringing theory and numerical results into close agreement.[10]

Figure 4 shows the average fraction $< f_s(K,I) >_I$ of the phase space occupied by stochastic orbits, obtained by averaging f_s over I for a given stochasticity parameter K. We have also plotted $< f_s(u) >_{u_l}^{u_{l-1}}$, the average fraction of the phase space occupied by stochastic orbits in the Fermi map. The average is taken over the action interval from the center of the island at $u_l = M/l$ to the center of the next island at $u_{l-1} = M/(l-1)$. This corresponds to $< f_s(K,I) >_I$ with $K = 2\pi M/u_l^2$. For greater accuracy in comparing the results of integrating the Fokker-Planck equation with numerical results, we have used $< f_s(u) >_{u_l}^{u_{l-1}}$ in calculating the diffusion coefficient (12). The resulting diffusion coefficient is shown in Fig. 5.

III. Use of the Diffusion Coefficient

The diffusion coefficient may be compared to numerical measurements obtained by direct iteration of the mapping equations. However it is difficult to make this comparison due to the rapid oscillations of the diffusion. In numerical calculations of D, we must iterate the map a number of times. As the

particles diffuse away from the initial action, they experience different local diffusions. In addition the friction coefficient B is non zero, which produces a net flux of particles in action, further complicating the comparison. Choosing large values of M increases the size of the stochastic region and the oscillation period of $D(u)$, yielding better agreement between the diffusion coefficient and the numerical calculations. But for sufficiently small values of u or sufficiently long iteration times, peaks and dips in the diffusion distort and change their positions in action, and the agreement is poor.

To account for these effects we integrate the Fokker-Planck equation using the theoretical diffusion coefficient (12) and a delta function at action u_o as an initial condition. This yields the predicted theoretical distribution function $f(u,n)$, where the dependence on the initial action u_o is suppressed. Recall, however, the existence of stable islands embedded in the stochastic sea. As discussed above, we expect that for times greater than the action evolution time, the total equilibrium distribution function $f_s(u,\psi) = \lim_{n\to\infty} f(u,\psi,n)$ will be uniform in those regions of phase space accessible to stochastic orbits.[9] When the integration over phase is performed to obtain $f_s(u)$, the islands will appear as dips. However, if we use the Fokker-Planck equation with (4), $\lim_{n\to\infty} f(u,n)$ will be constant for $u < u_b$. Therefore, the Fokker-Planck description must be modified to account for the islands. For example, to obtain $\lim_{n\to\infty} f(u,n) = f_s(u)$, Chirikov modifies (4) to[11]

$$B(u) = \frac{1}{2}\frac{\partial D(u)}{\partial u} + \frac{1}{2}D(u)\frac{d}{du}ln f_s(u) \qquad (13)$$

where $f_s(u)$ is obtained numerically. This procedure only ensures the correct invariant distribution, while we are interested in the short and intermediate

time behavior as well. Rather than modifying (4), we re-interpret $f(u,n)$. The information about the size and location of islands is contained in $f_s(u)$. To incorporate this information into the Fokker-Planck approach, we multiply $f(u,n)$ by $f_s(u)$ to obtain the observed distribution function:

$$F(u,n) = \frac{f(u,n)f_s(u)}{\int_o^{u_t} f(u',n)f_s(u')du'}. \tag{14}$$

Dividing by the integral ensures that the number of particles is conserved. Clearly as $n \to \infty$ and $f(u,n)$ becomes uniform, $F(u,n) \to f_s(u)$, which is in agreement with Chirikov's approach. However, for finite n, $F(u,n)$ will differ from the distribution obtained using (13). For example, initial conditions near a large island will result in large dips in $F(u,n)$ while the value obtained by use of (13) will be fairly smooth.

In addition to comparing $F(u,n)$ directly with distributions obtained by iterating the mapping equations, it is useful to calculate the second moment or variance of $F(u,n)$. This variance can be compared to the variance measured by iterating the map. That is, we compare the measured value of the variance σ_x^2 to the theoretical value

$$\sigma_t^2(u_o,n) = \frac{1}{n}\frac{\int \left(u - u_{ave}\right)^2 F(u,n)du}{\int F(u,n)du}, \tag{15}$$

where

$$u_{ave}(u_o,n) = \frac{\int uF(u,n)du}{\int F(u,n)du}.$$

We use u_{ave} rather than u_o in (15) because the friction may cause the entire distribution to drift. This would cause an anomalously large variance. The variance is a function of u_o through its dependance on the initial value used to calculate F.

We use a modified Crank-Nicolson method[12] to integrate the Fokker-Planck equation, with a small but finite width delta function in u as the initial distribution. The boundary conditions specify no flux at $u = 0$ and at $u = u_b$, where u_b is the action at the first KAM barrier that spans the phases in the (u, ψ) phase space. For the Fermi map $u_b \approx 2.5(\pi M/2)^{1/2} \approx 250$ for $M = 10,000$.

From (4) the diffusion (10) yields a friction coefficient (for $u << u_s$, where there are no significant stable islands)

$$B = \frac{\pi M}{u^3}\left(J_1\left(\frac{2\pi M}{u^2}\right) - J_3\left(\frac{2\pi M}{u^2}\right)\right) ,$$

which diverges as $O(1/u^2)$ for u small. This affects the convergence of the Crank-Nicolson method. To improve the convergence, the friction coefficient is set equal to zero for very small values of u, usually $u < 3$ or 4.

IV. Numerical Experiments

The mapping equations were solved numerically to see how well the theory corresponded to the actual dynamics. We followed m initial conditions (with m ranging from 1000 to 64000) having random initial phases at a fixed action $u = u_o$ for n between 1 and 1000 iterations. Figure 6 gives two examples of numerically obtained distribution functions. The action axis was divided into bins of width $\Delta u = .025$, and after iterating the map, the number of orbits residing in each bin was recorded. Thus each dot represents the number of particles within an interval Δu about a particular action. The solid lines are the predictions of the Fokker-Planck equation.

In Fig. 6a we note that the distribution is not symmetric due to the inhomogeneity of $D(u)$. The theory and experiment are in excellent agreement

regarding this fact. We note also that $F(u,n)$ is the same as the result obtained from (13) since there are no stable islands at this action. The bump in the distribution obtained in the numerical experiment at $100 < u < 105$ is due to particles in a small region of phase space streaming upward in action. This streaming behavior will be discussed below.

Figure 6b shows a region of action where large stable islands exist. Since there were no initial conditions inside the island centered at $u = 185$, the island manifests itself as a dip in the distribution function. Evidence of neighboring period one islands may be seen on the skirts of the distribution function at $u = 189$ and $u = 182$. The effects of the two iteration islands at $u = 183$ and $u = 187$ are also visible. The predictions of the Fokker-Planck equation using (13) and (14) are shown for comparison. We see that (14) agrees much better than (13) with the numerical results.

The variance was also calculated, using

$$\sigma_x^2(u_o,n) = \frac{1}{nm}\sum_{i=1}^{m}(u_i(n) - u_{ave})^2 \ . \tag{16}$$

The use of many initial conditions provides a way to estimate the error in the variance. We can calculate the variance for subgroups of $m_o < m$ initial conditions and then use the standard deviation as a measure of the uncertainty. Using $m = 64000$ initial conditions and $m_o = 16000$, a typical standard deviation is about one percent.

The results after an iteration time $n = 20$ are shown in Fig. 7a . The solid line is a linear interpolation of several hundred calculations of the variance, each at a different initial u_o. Each calculation was performed using the method

of Sec. III, that is, by integrating the Fokker-Planck equation and using (15). From now on the result (15) will be referred to as the theoretical variance.

The dots in Fig. 7a represent several hundred measurements of the variance using (16). The variances in Fig. 7a both show the characteristic oscillations observed in the standard map, for large values of the stochasticity parameter K. Both variances drop rapidly toward zero as K approaches one, as in the standard map. However, the oscillations occur in action space rather than in parameter space. For $u < 40$, both the theoretical and measured variances no longer exhibit oscillations. This is because as particles diffuse, they experience different local diffusions. The result is that rapid variations in $D(u)$ are averaged to the quasilinear value of 1/2.

We can estimate the limits of validity of quasilinear diffusion. We expect that quasilinear diffusion is adequate if large islands do not exist ($u < u_s$) and if particles diffuse over a range of action δu comparable to or larger than the local period of the oscillations in $D(u)$. For large K the diffusion oscillates as $\cos(K)$ so we expect averaging when $(\partial K/\partial u)\delta u \approx \pi/2$. Using $\delta u \equiv \sqrt{nD_{QL}}$ and

$$\frac{\partial K}{\partial u} = \frac{4\pi M}{u^3}$$

for the Fermi map, we find quasilinear diffusion for

$$u < (32M^2n)^{1/6} \leq u_s \,. \tag{17}$$

The validity of (17) has been studied numerically for $10^2 < M < 10^8$ and $10 < n < 1000$. For actions satisfying (17), the variance is within five percent of the quasilinear value.

Another effect of the variation of D with u is seen by comparing results of calculations made at different times n. Fig. 7b shows results at time $n = 40$. Comparing Fig. 7a to Fig. 7b, we see that the location of the maxima and minima of the variance change with n. Near $u = 75$ in Fig. 7b, a maximum and a minimum are merging, forming an irregular hump. Examination of Figs. 7a and 7b makes it clear that the maxima and minima of the variance do not always correspond to the maxima and minima of the diffusion coefficient in Fig. 5. These results are expected on physical grounds. As particles diffuse they experience different local diffusion rates. Particles starting near a local minimum diffuse into regions of higher diffusion rates. There they diffuse more rapidly than they would at the minimum, and thus the measured variance is greater than the local diffusion coefficient. A similar but opposite effect is seen near local maxima of D, reducing the variance. Particles starting between maxima and minima diffuse more rapidly toward regions of increasing D, thereby experiencing a friction given by (4).

For actions greater than $u \approx 200$, i.e. for actions near u_b, the numerically determined values of the variance exceed the theoretical values. Note, however, that the numerical value of the variance after 40 iterations is roughly half the value after 20 iterations. Any initial conditions started near the isolating KAM curve around a stable fixed point will tend to "stick" to the island border, being carried around the island. This effect will produce an anomalous variance which decays as $1/n$. As $n \to \infty$ we expect that the numerical variance will agree with the theoretical predictions. Numerically iterating the mapping equations for longer times verifies this $1/n$ decay. In calculating the variances, we have attempted to select only initial conditions outside of stable

islands. This is possible for period one fixed points, but for higher order fixed points our code was inadequate. Initial conditions started in such islands also produce variances which decay as $1/n$. These initial conditions do not produce long-time diffusion and therefore over sufficiently long times would lead to a numerical variance lower than that calculated from the Fokker-Planck equation, as observed numerically.

When we examine phase space portraits for initial conditions at these large actions (corresponding to K near K_{crit}), we see some interesting behavior. Particles diffuse rapidly up and down in action up to certain limits, beyond which they will not pass, at least initially. After repeated iterations particles will leak through these apparent barriers and again diffuse rapidly until they reach the next apparent barrier. This process repeats itself until the particles reach the isolating KAM curve at u_b, or until they diffuse toward lower actions where the behavior gradually passes into a more uniform diffusion.

Similar behavior has been described in a paper by Mackay, Meiss, and Percival.[13] They refer to these barriers as cantori. They give a theory describing the behavior and calculate a diffusion coefficient. By using the Fourier path diffusion coefficient we have averaged over a finite range of actions between primary resonances. In doing so, we have averaged the very slow "diffusion" across the cantorus with the much faster diffusion on either side.

The measured value of the variance also exceeds the theoretical value near values of u corresponding to $K = 2\pi M/u^2 = 2\pi l$ where l is an integer, and near $u = 145$ ($K = 2.95$). The standard map (8) exhibits "accelerator" modes near these values of K. An accelerator mode in the standard map is a stable fixed point of the map that corresponds to monotonic increase or decrease of

the action with each iteration of the map. Since the standard map is periodic in the action, these fixed points are encircled by KAM curves, and there is an "island of stability".[2] Orbits started inside the island remain inside and vice versa.

Locally, any small region of the Fermi map lying between adjacent (period one) island centers resembles the standard map. Thus, we expect the Fermi map to show behavior similar to that of accelerator modes in the standard map. However, generic maps such as the Fermi map are not periodic in the action. Because a change in u corresponds to a change in K, and accelerator modes in the standard map exist only for limited ranges of K, the Fermi map cannot have true accelerator modes. The corresponding fixed points and associated KAM curves do not exist. This allows orbits in the Fermi map to diffuse into and out of regions of phase space where they may be accelerated for a number of iterations that will depend on both K and M. Large values of M correspond to Fermi maps that closely resemble the standard map over many adjacent island centers, and thus exhibit orbits resembling accelerator modes for long times. An example of such behavior was seen in Fig. 6a near $u = 100$. The effect of such orbits on the variance is shown in Fig. 7a, where evidence of these "quasi-accelerator" modes may be seen at $u = 145.$ and $u = 100.$, corresponding to $K = 2.95$ and $K = 2\pi$. The effect of "quasi-accelerator" modes is the only major disagreement between our theory of diffusion and numerical experiments.

V. Conclusions

Using a local diffusion coefficient that includes the higher order correlations of diffusion in the standard map, the Fokker-Planck equation is integrated to obtain the evolution of the distribution function for stochastic orbits of generic Hamiltonian twist mappings. Oscillations of the variance as a function of the action are observed. For the Fermi map with $u < (32M^2n)^{1/6}$, these oscillations in the variance average to zero, yielding the quasilinear value. For larger values of u, the variance may exceed the quasilinear value by as much as a factor of two. For u approaching the KAM barrier, the variance tends to zero. In addition, peaks and dips in the diffusion interact in a complicated manner. These effects are predicted by the Fokker-Planck equation, using a local diffusion coefficient derived from a locally equivalent standard mapping.

Dips observed in the invariant (steady state) distribution are due to the existence of KAM barriers around stable fixed points. When these islands are taken into account the invariant distribution is homogeneous (to a good approximation), in agreement with the prediction of ergodic theory.

Acknowledgments

This work was supported by Office of Naval Research Contract N00014-79-C-0634 and National Science Foundation Grant ECS 8104561. The numerical work was done on the NMFECC computer network.

Appendix A: Derivation of the Local Diffusion Coefficient

In this appendix we derive a local, intermediate time, diffusion coefficient for radial twist mappings of the form

$$\begin{aligned} u_{n+1} &= u_n + \epsilon \sin\theta_n \\ \theta_{n+1} &= \theta_n + A(u_{n+1}) \ . \end{aligned} \tag{A1}$$

For the Fermi map our result will be equation (10).

Following Rechester et al.[3],[4] we introduce the Vlasov equation for the distribution function $P(\theta, u, t)$,

$$\frac{\partial P}{\partial t} + \frac{\partial \theta}{\partial t}\frac{\partial P}{\partial \theta} + \frac{\partial u}{\partial t}\frac{\partial P}{\partial u} - \frac{\sigma}{2}\frac{\partial^2 P}{\partial \theta^2} = 0 \ . \tag{A2}$$

We have introduced noise in the system, represented by the last term on the left hand side of (A2), corresponding to diffusion in θ with variance σ. Since we are interested in calculating an action diffusion coefficient, we let

$$P(\theta, u, t=0) = \frac{1}{2\pi}\delta(u - u_o) \ ,$$

that is, a line of initial conditions with random phases and initial action u_o. With this initial condition $P(\theta, u, t)$ is just the probabilistic form of the transition probability W_t used in the main text.

Equation (A2) may be solved using a Green's function. We find

$$P(\theta, u, t) = \int_o^{2\pi} G(\theta - \theta', u) P(\theta', u + \epsilon \sin\theta', t-1) d\theta', \tag{A3}$$

where

$$G(\theta - \theta', u) = \frac{1}{(2\pi\sigma)^{1/2}} \sum_{n=-\infty}^{\infty} \exp\left(-\frac{[\theta - \theta' - A(u) + 2\pi n]^2}{2\sigma}\right) \ . \tag{A4}$$

From the Poisson summation formula,[14] we have

$$\frac{1}{\lambda}\sum_{n=-\infty}^{\infty}\hat{\phi}\left(\frac{t+2\pi n}{\lambda}\right)=\sum_{m'=-\infty}^{\infty}\phi(\lambda m')e^{im't}$$

where $\hat{\phi}$ is the Fourier transform of ϕ. Choosing $\hat{\phi}(k)=\sqrt{\pi}e^{-k^2/4}$,

$$\hat{\phi}\left(\frac{t+2\pi n}{\lambda}\right)=\sqrt{\pi}\exp\left[-\left(\frac{t+2\pi n}{\sqrt{\sigma/2}}\right)^2/4\right],$$

with $\lambda=(\sigma/2)^{1/2}$. For $t=\theta-\theta'-A(u)$ we have

$$\frac{1}{(2\pi\sigma)^{1/2}}\sum_{n=-\infty}^{\infty}\exp\left(-\frac{[\theta-\theta'-A(u)+2\pi n]^2}{2\sigma}\right)$$
$$=\frac{1}{2\pi}\sum_{m'=-\infty}^{\infty}e^{\frac{-\sigma m'^2}{2}}e^{im'(\theta-\theta'-A(u))}.$$

Using this relation in (A4) and inserting into (A3), we obtain

$$P(\theta,u,t)=\sum_{m'=-\infty}^{\infty}e^{\frac{-\sigma m'^2}{2}}e^{im'\theta}e^{-im'A(u)}$$
$$\int_o^{2\pi}\frac{d\theta'}{2\pi}e^{-im'\theta'}P(\theta',u+\epsilon\sin\theta',t-1).$$

Introducing the Fourier transform of $P(\theta,u,t)$,

$$P(\theta,u,t)=\frac{1}{(2\pi)^2}\sum_m\int_{-\infty}^{\infty}dk\;e^{i[m\theta+ku]}a_m^t(k)$$
$$a_m^t(k)=\int_o^{2\pi}d\theta\int_{-\infty}^{\infty}du\;e^{-i[m\theta+ku]}P(\theta,u,t), \qquad \text{(A5)}$$

we find

$$a_m^t(k)=\sum_{m'=-\infty}^{\infty}e^{\frac{-\sigma m'^2}{2}}\int_o^{2\pi}d\theta\int_{-\infty}^{\infty}du\;e^{-i(m-m')\theta}e^{-iku}e^{-im'A(u)}$$
$$\int_o^{2\pi}\frac{d\theta'}{2\pi}e^{-im'\theta'}P(\theta',u+\epsilon\sin\theta',t-1).$$

Performing the θ integration yields a Kronecker delta, $\delta_{m,m'}$, and after doing the sum over m', we obtain

$$a_m^t(k) = e^{\frac{-\sigma m^2}{2}} \int_o^{2\pi} d\theta' \; e^{-im\theta'} \int_{-\infty}^{\infty} du \; e^{-i[ku+mA(u)]} P(\theta', u + \epsilon \sin\theta', t-1) \; . \tag{A6}$$

We now focus our attention on the u integral, treating θ' as fixed:

$$I_u = \int_{-\infty}^{\infty} du \; e^{-i[ku+mA(u)]} P(\theta', u + \epsilon \sin\theta', t-1) \; . \tag{A7}$$

As discussed in sec. I, we would like to describe the evolution of a distribution function in action alone, using the Fokker-Planck equation. Thus we are interested in calculating a diffusion coefficient for times t (Δn in sec. I) short enough that the action does not change by much, but long enough so that each particle in the distribution receives many uncorrelated kicks, i.e., we assume a separation of time scales $\tau_{action} >> t >> \tau_{phase}$. This means that in the expression for $a_m^t(k)$, t is short enough that $P(\theta', u + \epsilon \sin\theta', t-1)$ in (A7) is still sharply peaked. Because of this fact, we may expand $A(u)$ in the exponent around the initial action u_o:

$$\begin{aligned} A(u) =& A(u_o) + (u-u_o)\left(\frac{dA}{du}\right)_{u_o} + \frac{1}{2}(u-u_o)^2\left(\frac{d^2A}{du^2}\right)_{u_o} + \cdots \\ =& A(u_o) - u_o\left(\frac{dA}{du}\right)_{u_o} + u\left(\frac{dA}{du}\right)_{u_o} + \cdots \\ =& \alpha(u_o) + uK(u_o) + \cdots . \end{aligned} \tag{A8}$$

Then we obtain

$$I_u = e^{-im\alpha} \int_{-\infty}^{\infty} du \; e^{-i(k+mK)u} P(\theta', u + \epsilon \sin\theta', t-1) \; .$$

Letting $w = u + \epsilon \sin\theta'$, we see that

$$I_u = e^{-im\alpha} e^{i\epsilon(k+mK)\sin\theta'} \int_{-\infty}^{\infty} dw \; e^{-i(k+mK)w} P(\theta', w, t-1) \; .$$

Using this in (A6) we obtain

$$a_m^t(k) = \sum_{l=-\infty}^{\infty} J_l(|k'\epsilon|)e^{\frac{-\sigma m^2}{2}}e^{-im\alpha}$$
$$\int_o^{2\pi} d\theta' \int_{-\infty}^{\infty} dw\ e^{-i[(m-l\mathrm{sgn}(k+mK))\theta'+(k+mK)w]}P(\theta', w, t-1)\ .$$

where we have also used the identity

$$e^{\pm i\beta\sin\theta} = \sum_{l=-\infty}^{\infty} J_l(\beta)e^{\pm il\theta}\ ,\quad \beta > 0\ .$$

Using the definition (A5) in the double integral, but at time $t-1$, we obtain the recursion relation

$$a_m^t(k) = \sum_{l=-\infty}^{\infty} J_l(|k'\epsilon|)e^{\frac{-\sigma m^2}{2}}e^{-im\alpha}a_{m'}^{t-1}(k') \qquad \text{(A9)}$$

where

$$k' = k + mK$$
$$m' = m - l\mathrm{sgn}k'\ .$$

This result differs from that in reference (4) by the term $e^{-im\alpha}$ in (A9), and by the expression for k'. The difference in k' results in a change in the arguments of the Bessel functions. In the case of the standard map k is an integer. In the more general case k is K times an integer (or zero).

With (A9) we can obtain the diffusion coefficient from the following argument[4,7] . Using equation (A5) in the definition of the diffusion coefficient (2) and integrating by parts, we find

$$D(u_o) = \lim_{k\to 0^+} -\frac{1}{T}\frac{\partial^2}{\partial k^2}a_o^T(k)\ , \qquad \text{(A10)}$$

where $T >> \tau_{phase}$, and we have neglected terms proportional to $1/T$. From this expression we see that the path in Fourier space must end at $(m,k) = (0,0)$.

Furthermore, we are interested in the case $\epsilon K \geq .9716$, that is, where diffusion occurs in the absence of external noise. In this case $T >> (2/K\epsilon)^2$ and the path must also begin at $(0,0)$.[4] Because the path must begin and end at (m,k) the sum $\sum_t m_t = 0$. Therefore $\prod_t e^{-im_t\alpha} = 1$, so that the $e^{-im\alpha}$ term in (A9) has no effect on the diffusion coefficient. If each m in the recursion (A9) is equal to zero, then

$$a_m^T(k) = [J_o(|k\epsilon|)]^T a_o^o(k)$$

and from (A10), treating $k\epsilon$ as small, $J_o(|k\epsilon|) \approx 1 - (k\epsilon/2)^2$ so that

$$D(u_o) = \epsilon^2/2 .$$

Considering now paths that leave the origin we see from (A9) that for the first step away from $(0,0)$, $m' = -l\text{sgn}k'$ and $k' = k$. That is, the first step must be $(0,0) \rightarrow (-l\text{sgn}k', 0)$, from which we obtain a factor $J_l(|k\epsilon|)$, where k tends to zero. Furthermore, since the path must end at the origin we must have a step $(l, -lK) \rightarrow (0,0)$, giving a factor $J_l(|k\epsilon|)$. For k small, $J_l(k\epsilon) \approx (k\epsilon/2)^l$. These steps will contribute a factor of k^{2l}, which will give a zero contribution to the diffusion unless $l = \pm 1$ and one derivative in (A10) operates on each $J_l(|k\epsilon|)$. These two steps will contribute a factor of $\epsilon^2/4$ to each path that leaves the origin. The simplest example of a path which leaves the origin is given by $(0,0) \rightarrow (1,0) \rightarrow (-1,K) \rightarrow (0,0)$, (and its mirror image), which gives

$$a_m^t(k) = 2(T-2)\,[J_o(|k\epsilon|)]^{T-3} J_{-1}(|k\epsilon|) J_2(|(k+K)\epsilon|) e^{-\sigma/2} J_1(|k\epsilon|) e^{-\sigma/2},$$

and contributes a term

$$-\epsilon^2 J_2(|K\epsilon|) e^{-\sigma}$$

to the diffusion.

We may proceed in this manner to sum more paths to obtain more accurate values of $D(u_o)$. But notice that whenever ϵ appears in the argument of a Bessel function, it will always be multiplied by $k' = k + mK$. Bessel functions with $m = 0$ contribute factors of $J_o(0) = 1$, $J_l(0) = 0$, or $\epsilon/2$, where the last term corresponds to entering or leaving the origin. Because of this simple rule, we may take over the results of reference (4) simply by letting $\epsilon \to K\epsilon$. However, we must divide the result by K^2 to cancel the extra K^2 in $(\epsilon/2)^2 \to (\epsilon K/2)^2$ corresponding to the steps entering and leaving the origin. This must also be done for the path which does not leave the origin. Symbolically,

$$D(u_o) = \frac{1}{K^2} D_\infty(\epsilon K),$$

where $K = (\partial A/\partial u)_{u_o}$. For maps such as the Fermi map, $\epsilon = 1$, and

$$D(u_o) = \frac{1}{K^2} D_\infty(K) \, .$$

which is equation (10). For the Fermi map, $A(u) = 2\pi M/u$, so that $K(u_o) = -2\pi M/u_o^2$, and if $K >> 1$ we obtain

$$D(u_o) = \frac{1}{2} - J_2\left(\frac{2\pi M}{u_o^2}\right) + J_2^2\left(\frac{2\pi M}{u_o^2}\right) \, ,$$

which is equation (11).

For the expansion (A8) to be valid, we must have

$$(u - u_o)\frac{\partial A}{\partial u} >> \frac{1}{2}(u - u_o)^2 \frac{\partial^2 A}{\partial u^2} \, ,$$

or

$$K \Big/ (\partial K/\partial u) >> \frac{1}{2}(u - u_o) \, . \qquad \text{(A11)}$$

As an estimate we have $|u - u_o| \approx \epsilon\sqrt{T}$, using the quasilinear diffusion. For the Fermi map (A11) becomes

$$u_o >> \sqrt{T}$$

which is usually easily satisfied.

Appendix B: Island Size Calculation

We outline here the perturbation calculation for the size of the stable islands in the standard map.

First we convert the standard map to a Hamiltonian. Using a periodic delta function,

$$\sum_{q=-\infty}^{\infty} \delta(n-q) = \sum_{q=-\infty}^{\infty} \cos(2\pi q n)$$

where n is the "time", the map may be written in the Hamiltonian form

$$H(I,\theta;n) = \frac{1}{2}I^2 + K\sum_{q=-\infty}^{\infty} \cos(\theta - 2\pi n q).$$

Moving to extended phase space, we obtain

$$\tilde{H}(I,\theta,J,\phi) = 2\pi J + \frac{1}{2}I^2 + K\sum_{q=-\infty}^{\infty} \cos(\theta - \phi q),$$

where $J = -H/2\pi$ and $\phi = 2\pi n$. The new Hamiltonian is independent of the new "time" ξ. Letting $\theta \to \pi + \theta$, we find the Hamiltonian for a driven pendulum

$$\begin{aligned}\tilde{H} = \frac{1}{2}I^2 + 2\pi J - K\cos\theta \\ - K\sum_{q\neq 0}\cos(\theta - q\phi).\end{aligned} \tag{B1}$$

We have a slow motion described by the (I,θ) variables and a fast motion described by the (J,ϕ) variables. Near the pendulum separatrix, the interaction between the two oscillations leads to chaotic motion and jumps in the actions I and J. The jump in J may be calculated over a half-period of the separatrix

motion. Since $\tilde{H}$ is linear in J we may write $\phi(t) = \Omega t + \Phi_o$, where $\Omega = 2\pi$ is the period of the J motion and Φ_o is an initial phase. For $\theta(t)$ we use the expression for θ on the separatrix: $\theta(t) = 4\tan^{-1} e^{-\omega_o t} - \pi$. Keeping only the leading term in the interaction we obtain

$$\begin{aligned}\Delta J &= -\int dt \frac{\partial \tilde{H}}{\partial \phi} \\ &= K \sin\Phi_n \int_{-\infty}^{\infty} \frac{d\tau}{\omega_o} \cos\left(\theta(\tau) + \Omega\frac{\tau}{\omega_o}\right) \\ &= \frac{K}{\omega_o} A_2\left(\frac{\Omega}{\omega_o}\right) \sin(\Phi_n)\end{aligned}$$

where Φ_n is the phase after n half-periods and $\omega_o = \sqrt{K}$ is the period of small librations of the pendulum. The maximum amplitude of the jump is thus $\Delta J_o = (K/\omega_o)\, A_2\,(\Omega/\omega_o)$, where the Melnikov-Arnold integral $A_2(Q_o)$ is given by

$$A_2(Q_o) = \frac{4\pi Q_o \exp\left(\pi Q_o/2\right)}{\sinh(\pi Q_o)} .$$

The change in the phase Φ is ΩT, where

$$T = (1/\omega_o) \ln\left(\hat{32} \Big/ \left|\frac{H-K}{K}\right|\right)$$

is the half-period of the motion near the separatrix. These relations may be expressed as a mapping (called the separatrix map[2]),

$$\begin{aligned} w_{n+1} &= w_n - \frac{\Omega \Delta J_o}{K} \sin\Phi_n \\ \Phi_{n+1} &= \Phi_n + \frac{\Omega}{\omega_o} \ln\frac{32}{|w_{n+1}|} \end{aligned} \qquad \text{(B2)}$$

where $w(J) = (H-K)/K$, which is the deviation of the energy $H = -\Omega J$ from its value of K on the separatrix. The width of the stochastic layer in the separatrix map corresponds to the width of the separatrix around the resonance

in the standard map. This width is found by using the 2/3 rule[7] or by approximating the separatrix map by the standard map and solving $K(w_b) = K_{crit}$. The result is

$$w_b = \frac{\Omega}{\omega_o}\frac{\Omega\Delta J_o}{K}$$
$$= \frac{\Omega^2}{K} A_2\left(\frac{\Omega}{\omega_o}\right) .$$

We then use $J = -K(1+w)/\Omega$, and the sign of w_b that describes the separatrix widening into the island to obtain

$$J_b = -\frac{K}{\Omega} + \Omega A_2\left(\frac{\Omega}{\omega_o}\right).$$

Returning to the Hamiltonian (B1), we solve for $I = I_b(\theta)$. This is the equation of the outer-most stable orbit which determines the size of the island:

$$\tilde{H} = \Omega J_b + \frac{1}{2} I_b^2 - K\cos\theta$$

or, since $\tilde{H} \equiv 0$,

$$I_b^2(\theta) = 2K\cos\theta + 2K - 2\Omega^2 A_2\left(\frac{\Omega}{\omega_o}\right)$$
$$= 2K(1+\cos\theta) - \frac{64\pi^4}{K^{\frac{1}{2}}}\frac{\exp\left(\frac{\pi^2}{\sqrt{K}}\right)}{\sinh\left(\frac{2\pi^2}{\sqrt{K}}\right)} .$$

To apply this result to the Fermi map, we note that $K(u_o) = 2\pi M/u_o^2$ and $\Delta u = (1/K)I$ so that

$$\Delta u_b(\theta) = \sqrt{\frac{2}{K}(1+\cos\theta) - \frac{64\pi^4}{K^{5/2}}\frac{\exp(\pi^2/\sqrt{K})}{\sinh(2\pi^2/\sqrt{K})}}.$$

This is the equation of the island surrounding the stable fixed point at $u_o = M/l$, where l is an integer.

The calculation of the size of the islands surrounding period two fixed points is similar. We start with the same Hamiltonian:

$$\begin{aligned}\tilde{H}(I,\theta,J,\phi) &= \frac{1}{2}I^2 + 2\pi J + K\sum_{q=-\infty}^{\infty}\cos(\theta - q\phi) \\ &= \tilde{H}_o + \tilde{H}_1\end{aligned} \tag{B3}$$

with $\tilde{H}_o = (1/2)I^2 + 2\pi J$ and $\tilde{H}_1 = K\sum_{q=-\infty}^{\infty}\cos(\theta - q\phi)$. We are interested in zero order orbits at $I = (2p+1)\pi$ and $\theta = In$, so that

$$\frac{\omega_1}{\omega_2} = \frac{2p+1}{2}.$$

We see that $\tilde{H}_1$ has no first order resonances. Since the perturbation term in (B3) does not exhibit this resonance in lowest order, the calculation must be carried out to second order. It is therefore convenient to use Lie transformation methods[7] to obtain the analog of B1. We wish to obtain a canonical transformation $w(I,\theta,J,\phi)$ to a new Hamiltonian K_T that has no oscillatory part (along the zero order orbits). We do this by solving the following set of equations:

$$\begin{aligned}0 &= K_o - \tilde{H}_o \\ D_o w_1 &= K_1 - \tilde{H}_1 \\ D_o w_2 &= 2(K_2 - \tilde{H}_2) - \left[w_1, (\tilde{H}_1 + K_1)\right]\end{aligned} \tag{B4}$$

and so on. Here $D_o w = \frac{\partial}{\partial \xi} + \left[w, \tilde{H}_o\right]$ where $[\ ,\ ]$ is the Poisson bracket in extended phase space. We pick K_1 to eliminate secular terms on the right-hand side of the first order equation. Then w_1 is chosen to solve the resulting equation. We then use w_1 in the second order equation and follow the same procedure to find K_2 and w_2. The new Hamiltonian K_T describes the motion near the period two fixed point at $I = (2p+1)\pi$.

Since $K_1 = < \tilde{H}_1 >$, we have $K_1 = 0$. Solving for w_1, we obtain

$$[w_1, \tilde{H}_o] = \left(I\frac{\partial}{\partial\theta} + 2\pi\frac{\partial}{\partial\phi} \right) w_1$$
$$= -K \sum_{q=-\infty}^{\infty} \cos(\theta - q\phi) ,$$

such that

$$w_1 = -K \sum_{q=-\infty}^{\infty} \frac{sin(\theta - q\phi)}{I - 2\pi q} .$$

We note that the denominator is non resonant. Proceeding to second order, we have $\tilde{H}_2 = 0$, so that the right-hand side of (B4) is $-[w_1, \tilde{H}_1]$. We choose K_2 to eliminate $1/2 < [w_1, \tilde{H}_1] >$, where $< >$ denotes averaging over θ:

$$K_2 = -\frac{1}{2} \left\langle \frac{\partial w_1}{\partial I} \frac{\partial \tilde{H}_1}{\partial \theta} \right\rangle$$
$$= \frac{K^2}{2} \left\langle \sum_{q,q'} \frac{\sin(\theta - q\phi) \sin(\theta - q'\phi)}{(I - 2\pi q)^2} \right\rangle$$
$$= \frac{K^2}{2} \left\langle \sum_{q,q'} \frac{\cos(q - q')\phi - \cos[2\theta - (q + q')\phi]}{(I - 2\pi q)^2} \right\rangle .$$

Performing the sums and averaging, we find

$$K_2 = \frac{K^2}{16} - \frac{K^2}{16} \cos[2\theta - (2p + 1)\phi] .$$

The transformed Hamiltonian (including the averaged terms) is then

$$K_T = \frac{1}{2} I^2 + 2\pi J - \frac{K^2}{16} \cos[2\theta - (2p + 1)\phi]$$
$$+ K \sum_q \cos(\theta - q\phi) - \frac{K^2}{4} \sum_{q+q' \neq 2p+1} \frac{\cos[2\theta - (q + q')\phi]}{(I - 2\pi q)^2} .$$

To put K_T in the form of a driven pendulum we use

$$F_2 = (2\theta - (2p + 1)\phi) J_1 + \phi J_2$$

to make a final transformation $I = 2J_1$, $J = J_2-(2p+1)J_1$, $\theta_1 = 2\theta-(2p+1)\phi$, $\theta_2 = \phi$. Expanding to second order around the fixed point at $J_{1o} = (\pi/2)(2p+1)$, we find

$$\Delta K_T(J_1,\theta_1,J_2,\theta_2) = \frac{1}{2}4(\Delta J_1)^2 + 2\pi J_2 - \frac{K^2}{16}\cos\theta_1 + K\sum_q \cos\left(\frac{1}{2}\theta_1 + (p-q+\frac{1}{2})\theta_2\right) - \frac{K^2}{16\pi^2}\sum_{q+q'\neq 2p+1}\frac{\cos\left[\theta_1 + ((2p+1)-(q+q'))\theta_2\right]}{(p-q+\frac{1}{2})^2}.$$

The rest of the calculation exactly parallels that given after (B1). For the Hamiltonian ΔK the frequency of small librations is $\omega_o = K/2$, and there are two types of perturbations. The dominant term is $K\cos\Big((1/2)\theta_1 - (1/2)\theta_2\Big)$. This calculation gives an estimate for the equation of the stable island

$$I_b(\theta) = \sqrt{\frac{K^2}{8}(1+\cos\theta) - \frac{32\pi^2}{K}\frac{\exp(\frac{\pi^2}{K})}{\sinh(\frac{2\pi^2}{K})}}.$$

For the island size around the $u = 2M/(2p+1)$ fixed point of the Fermi map we find

$$\Delta u_b = \sqrt{\frac{1}{8}(1+\cos\theta) - \frac{32\pi^3}{K^3}\frac{\exp(\frac{\pi^2}{K})}{\sinh(\frac{2\pi^2}{K})}}.$$

The results of these calculations are shown as the solid lines in Fig. 3.

References

[1]M.A. Lieberman and A.J. Lichtenberg, *Phys. Rev. A* **5** 1852 (1972)

[2]B. V. Chirikov, *Phys. Rep.* **52**, No. 5 263 (1979)

[3]A. B. Rechester and R. B. White, *Phys.Rev.Lett.* **44** 1586 (1980)

[4]A. B. Rechester, M. N. Rosenbluth, and R. B. White, *Phys.Rev.A* **23** 2664 (1981)

[5]M. C. Wang, G.E. Uhlenbeck, *Rev. Mod. Phys.* **17** 523 (1945)

[6]L. D. Landau, *Zh. Eksper. Theor. Fiz.* **7** 203 (1937)

[7]A. J. Lichtenberg and M. A. Lieberman, *Regular and Stochastic Motion* Springer-Verlag New York (1983)

[8]A. B. Rechester and R. B. White, private communication.

[9]V. I. Arnold, and A. Avez, *Ergodic Problems of classical Mechanics* Benjamin, New York (1968)

[10]A. J. Lichtenberg, DRFC-STGI (Fontenay-aux-Roses) preprint no. EUR-CEA-FC-1215 Dec. (1983), to be published in *Nuclear Fusion*

[11]B. V. Chirikov, Inst. of Nucl. Phys. preprint no. 182-132 Aug. (1982)

[12]L. W. Johnson, and R. D. Riess, *Numerical Analysis* Addison-Wesley Reading, Massachusetts (1982)

[13]R. S. Mackay, J. D. Meiss, and I. C. Percival, *Physica D* **13D** 55 (1984)

[14]I. Stackgold *Green's Functions and Boundary Value Probems* John Wiley and Sons, New York (1979)

Figure Captions

Fig. 1. The Fermi map for $M = 10,000$. Thirty-two initial conditions started near $u = 10$ were iterated 1,400,000 times; u_b marks the KAM barrier and u_s the stochastic barrier. Twenty initial conditions were started above u_b and iterated 200 times to illustrate regular orbits.

Fig. 2. $D_\infty(K)$ vs. K, from A. B. Rechester and R. B. White, private communication.

Fig. 3. The equilibrium distribution function obtained from 10 million iterations of 64 initial conditions started at low initial velocities. The phase space is projected onto the action axis, which is divided into 6000 bins. The dots represent the (normalized) number of visits to each bin. The solid lines are the fraction of phase space outside stable islands, as calculated in the appendix.

Fig. 4. The (averaged) fraction of the area accessible to stochastic orbits in the Fermi map, $< f_s(u) >_{u_i}^{u_{i-1}}$, and in the standard map, $< f_s(K,I) >_I$. The deviation for large u is due to insufficient iteration time in the Fermi map.

Fig. 5. The local diffusion coefficient given in (12) as a function of action, u.

Fig. 6. (a) The distribution function obtained by iterating 6400 initial conditions with $u_o = 90$ and random phases. The dots indicate the number of particles within $\Delta u = .025$ at a given action. The solid line is the prediction of the Fokker-Planck equation with the diffusion coefficient (12); (b) The same as (a), with $u_o = 186$. The dashed line is obtained using (13).

Fig. 7. The variance plotted as a function of initial action. Each dot corresponds to a measurement of the diffusion obtained by iterating the Fermi map. The solid line is the theoretical variance obtained by integrating the Fokker-Planck equation; (a) after 20 iterations; (b) after 40 iterations.

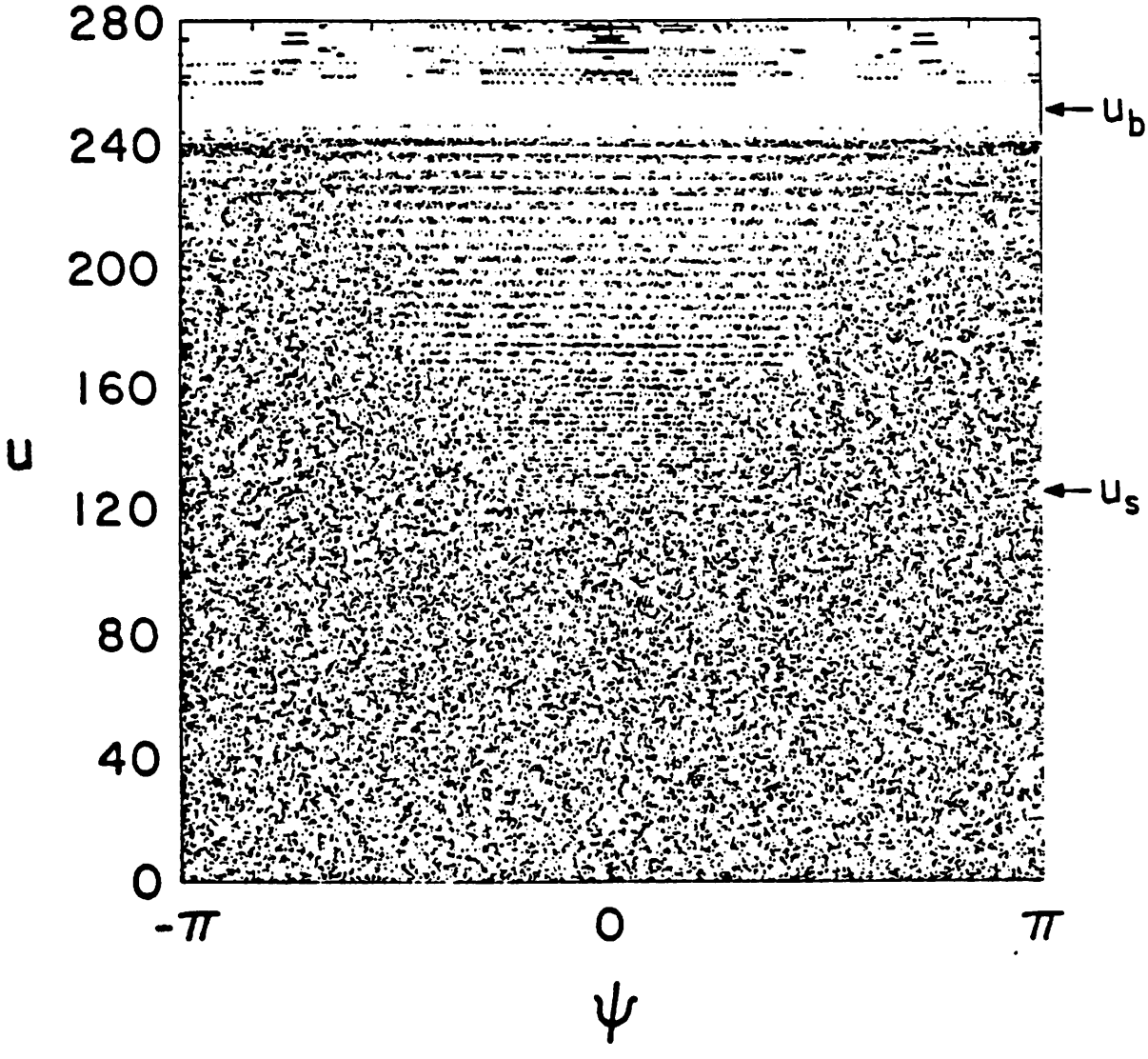

Fig. 1

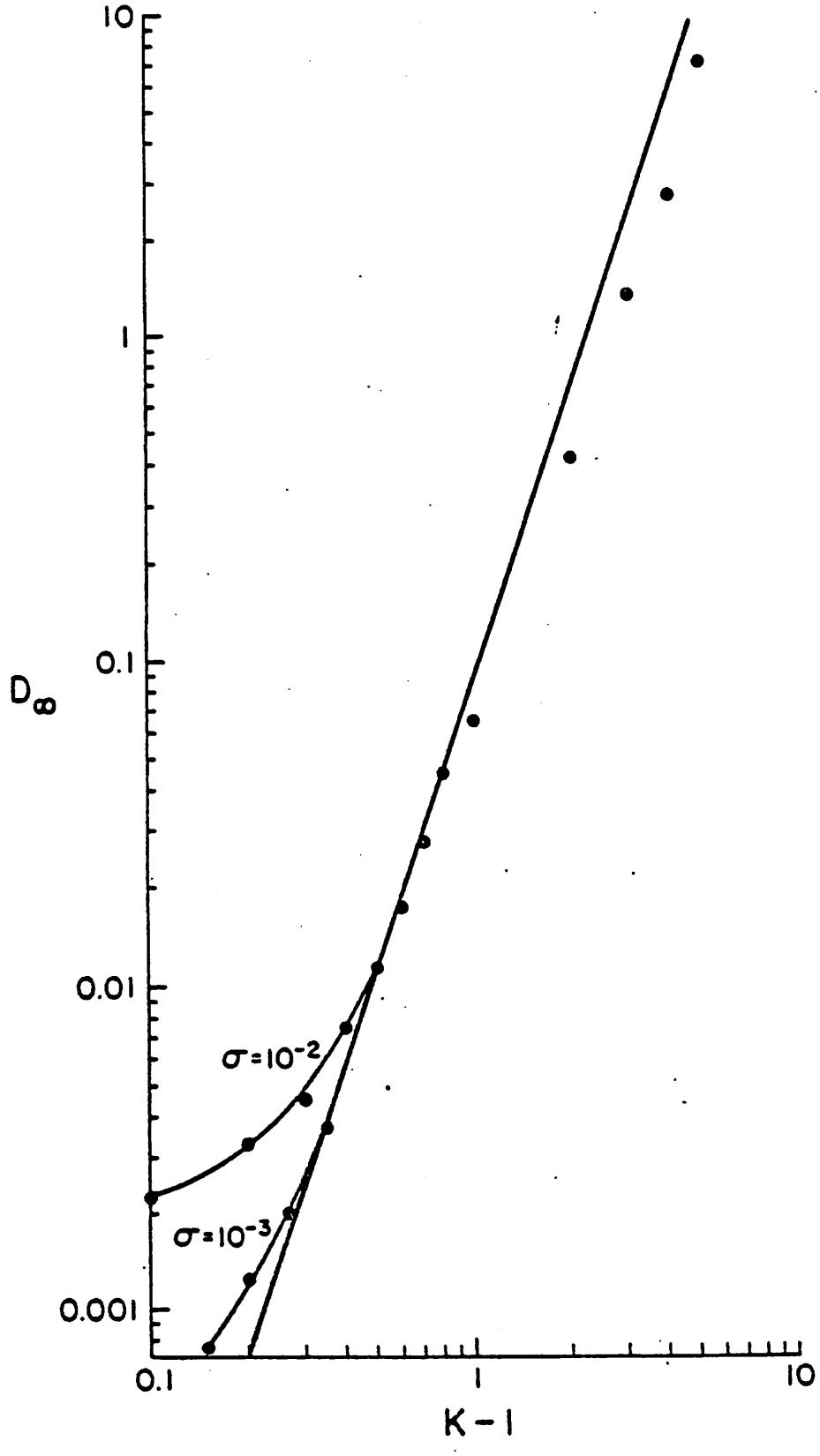

Fig. 2

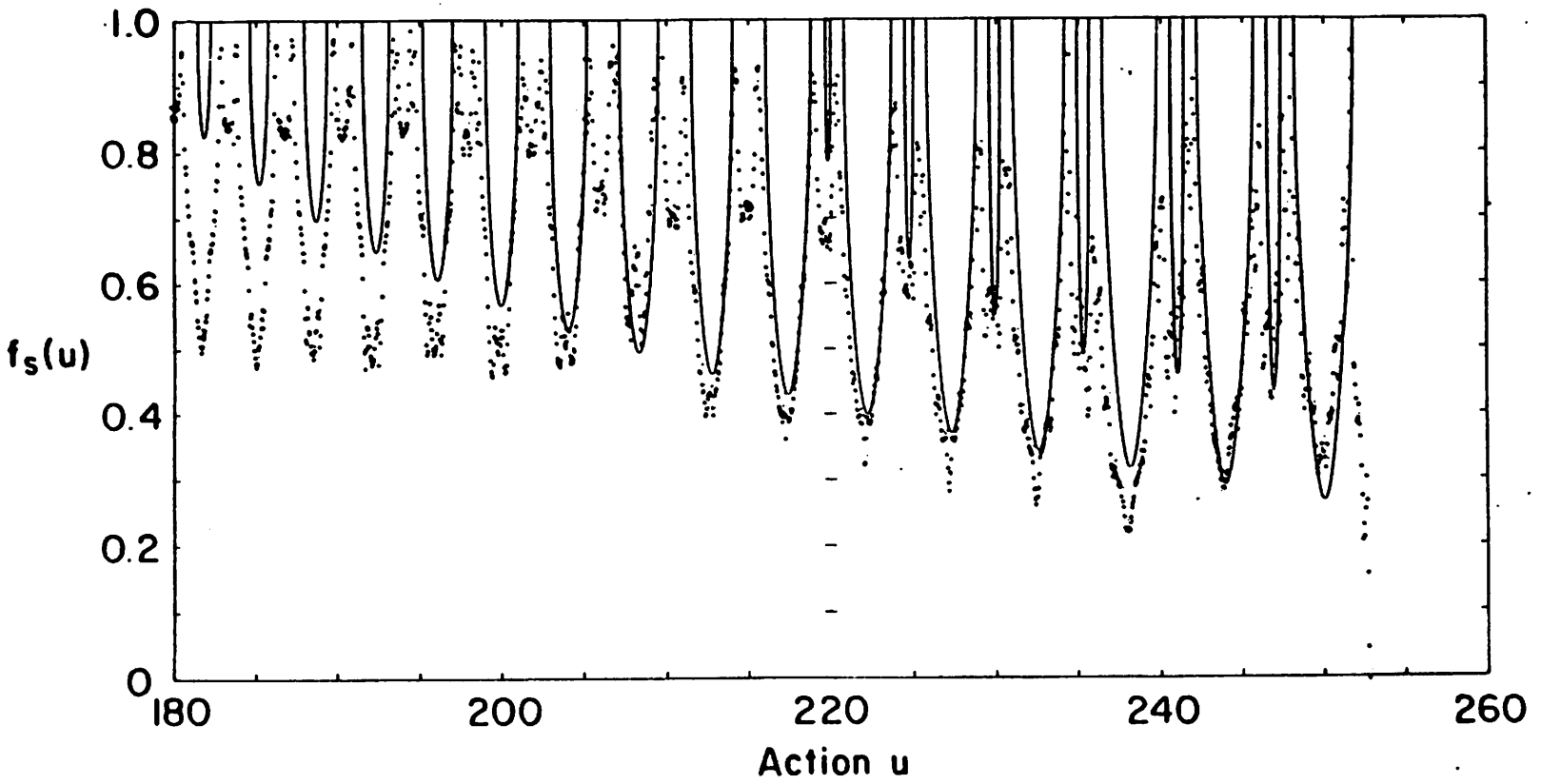

Fig. 3

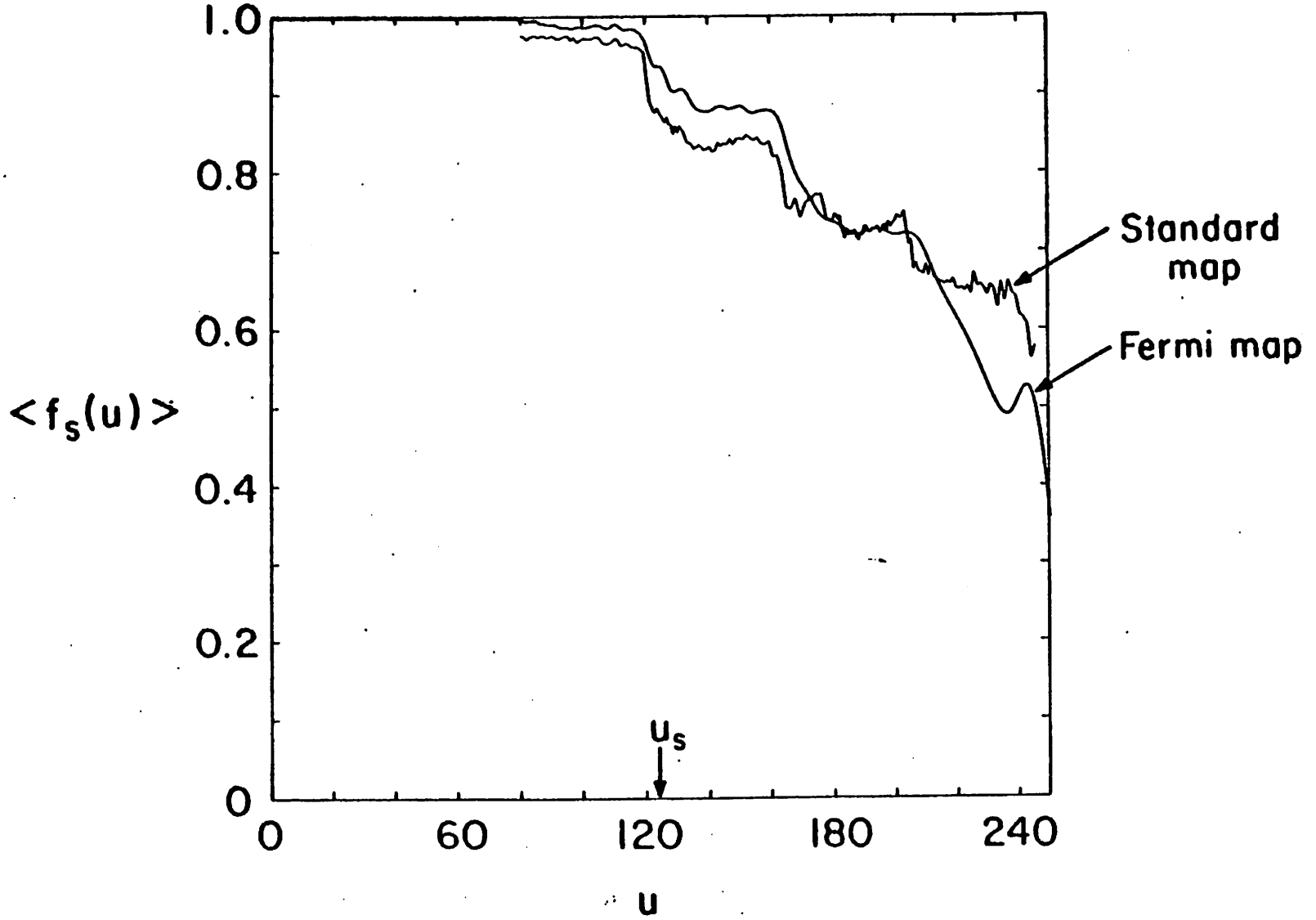
1.0
0.8
0.6
0.4
0.2
0
$\langle f_s(u) \rangle$
Standard map
Fermi map
u_s
0
60
120
180
240
u

Fig. 4

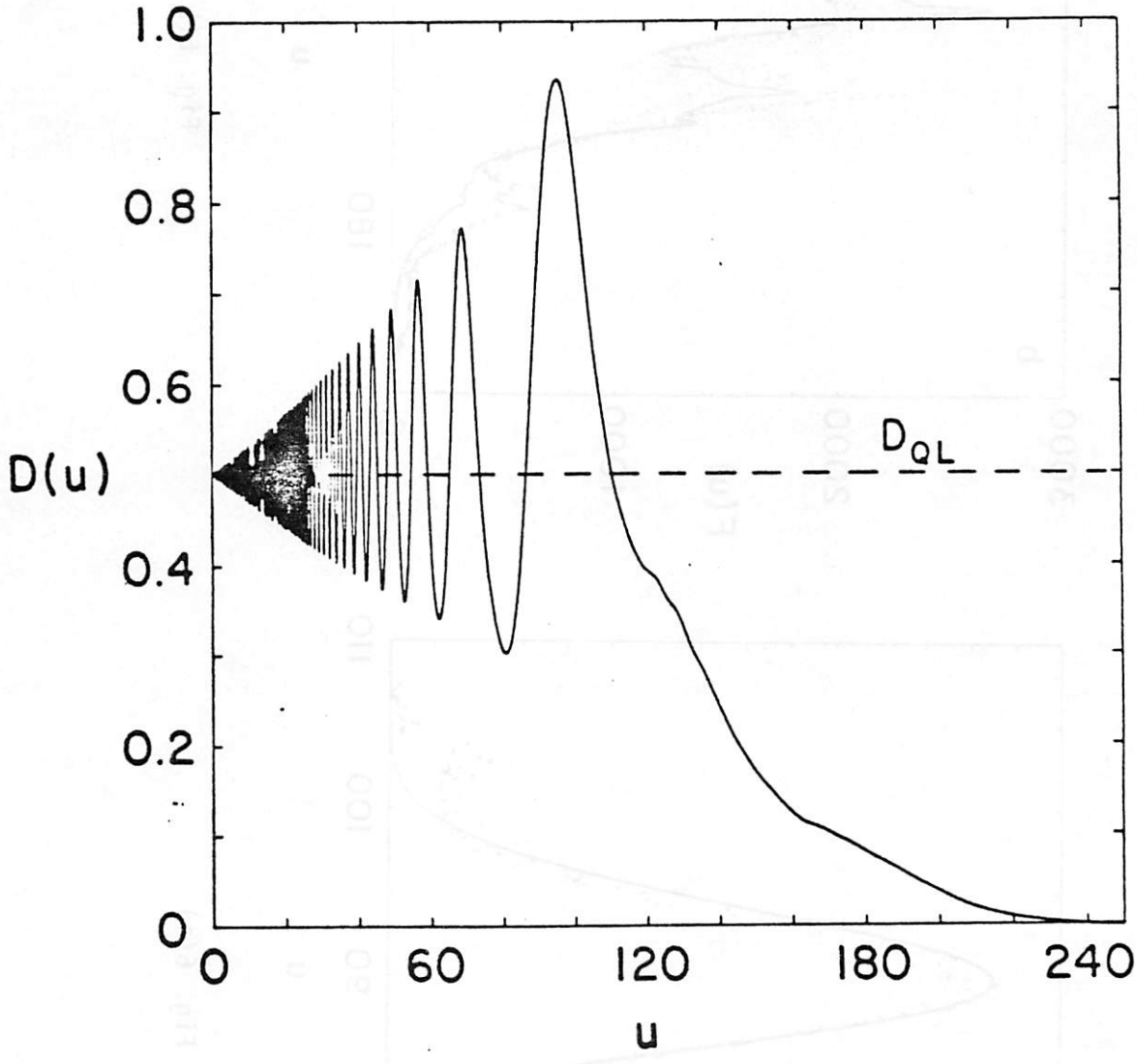

Fig. 5

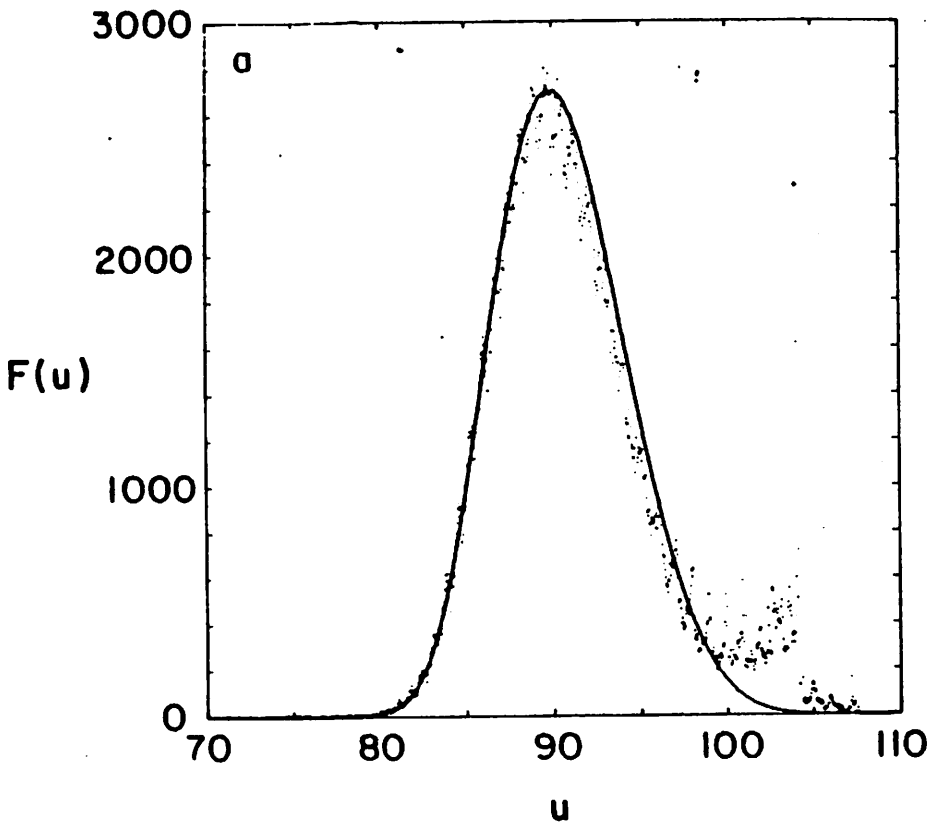
a
3000
2000
1000
0
F(u)
70
80
90
100
110
u

Fig. 6(a)

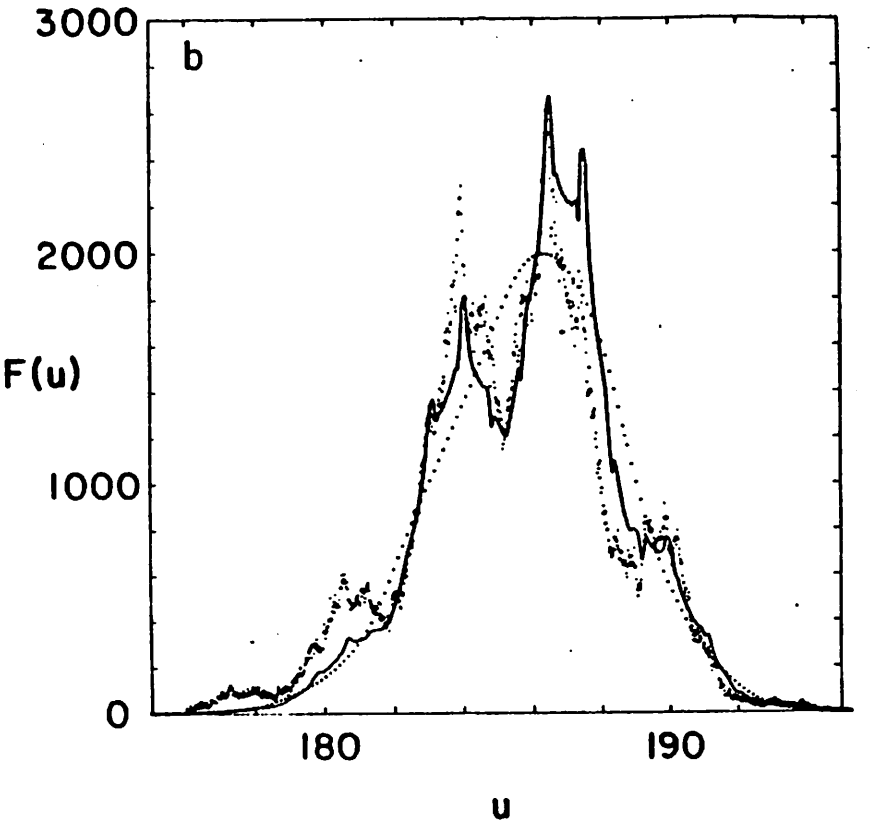
b
3000
2000
1000
0
F(u)
180
190
u

Fig. 6(b)

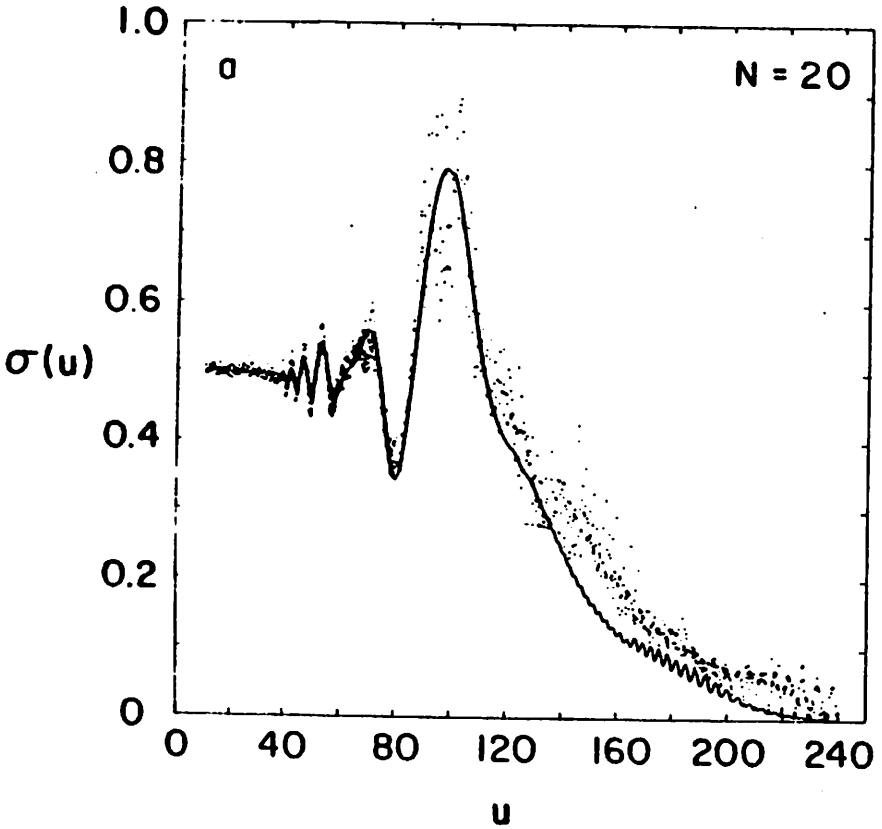
a
N = 20
1.0
0.8
0.6
0.4
0.2
0
σ(u)
0
40
80
120
160
200
240
u

Fig. 7(a)

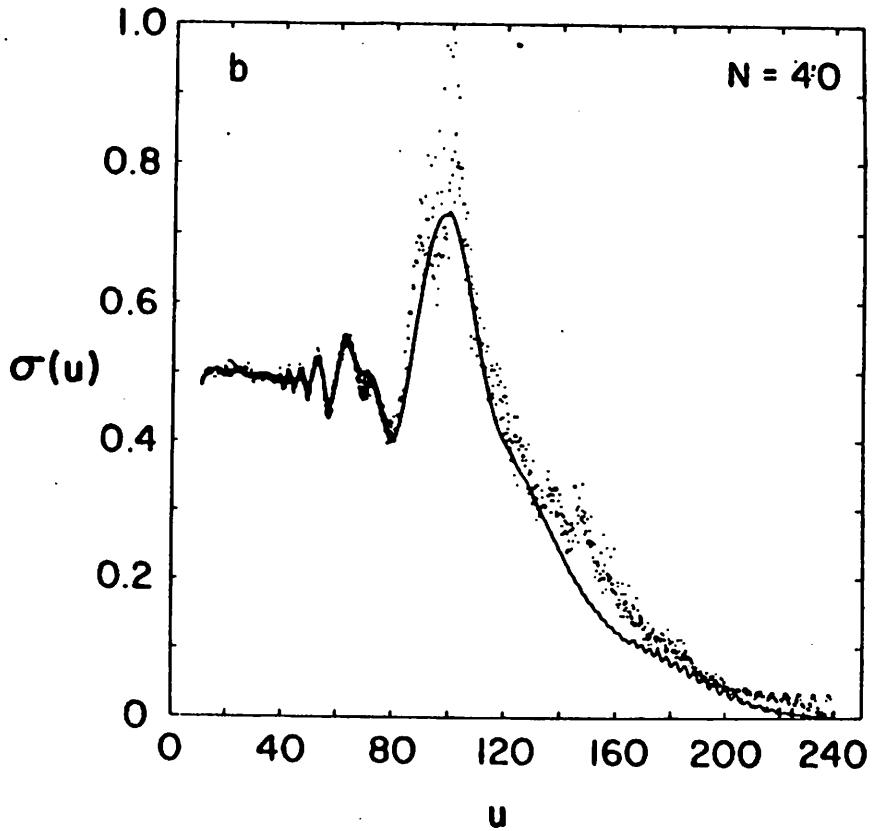
b
N = 40
1.0
0.8
0.6
0.4
0.2
0
σ(u)
0
40
80
120
160
200
240
u

Fig. 7(b)